Advances in Nano Research, *Vol. 15, No. 1 (2023) 35-48*
https://doi.org/10.12989/anr.2023.15.1.035

Sol-gel synthesis, computational chemistry, and applications of Cao nanoparticles for the remediation of methyl orange contaminated water

Nnabuk Okon Eddy*[1], Rajni Garg[2], Rishav Garg[3], Samson I. Eze[1], Emeka Chima Ogoko[4], Henrietta Ijeoma Kelle[4], Richard Alexis Ukpe[5], Raphael Ogbodo[6] and Favour Chijoke[1]

[1]*Department of Pure and Industrial Chemistry, University of Nigeria, Nsukka, Enugu State, Nigeria*
[2]*Department of Applied Sciences, Galgotias College of Engineering & Technology, Greater Noida, Uttar Pradesh 201310, India*
[3]*Department of Civil Engineering, Galgotias College of Engineering & Technology, Greater Noida, Uttar Pradesh 201310, India*
[4]*Department of Chemistry, National Open University of Nigeria, National Headquarter, Jabbi, Abuja, Nigeria*
[5]*Department of Chemistry, Federal University, Otuoke, Bayelsa State, Nigeria*
[6]*Department of Chemistry, University of Iowa, Iowa City, 52244 Iowa, USA*

(*Received January 2, 2022, Revised January 3, 2022, Accepted January 9, 2023*)

Abstract. Nanoparticles are known for their outstanding properties such as particle size, surface area, optical and electrical properties. These properties have significantly boasted their applications in various surface phenomena. In this work, calcium oxide nanoparticles were synthesized from periwinkle shells as an approach towards waste management through resource recovery. The sol gel method was used for the synthesis. The nanoparticles were characterized using X-Ray diffractometer (XRD), Fourier Transformed Infra-Red Spectrophotometer (FTIR), Brunauer Emmett Teller (BET), scanning electron microscopy (SEM), transmission electron microscopy (TEM) and ultra violet visible spectrophotometer (UV-visible). while DLS and SEM underestimate the particle diameter, the BET analysis reveals surface area of 138.998 m^2/g, pore volume = 0.167 m^3/g and pore diameter of 2.47 nm. The nanoparticles were also employed as an adsorbent for the purification of dye (methyl orange) contaminated water. The adsorbent showed excellent removal efficiency (up to 97 %) for the dye through the mechanism of physical adsorption. The adsorption of the dye fitted the Langmuir and Temkin models. Analysis of FTIR spectrum after adsorption complemented with computational chemistry modelling to reveal the imine nitrogen group as the site for the adsorption of the dye unto the nanomaterials. The synthesized nanomaterials have an average particle size of 24 nm, showed a unique XRD peak and is thermally and mechanically stable within the investigated temperature range (30 to 70 °C).
Keywords: adsorption; calcium oxide nanoparticles; methyl orange; periwinkle shell; resource recovery; solid waste

1. Introduction

One of the fundamental benefits of modern science is the initiative of managing natural resources for the benefit of the environment. The disposal of solid wastes is a global challenge considering their slow rate of decomposition. Unfortunately, the greatest volume of most industrial and domestic wastes falls into this class (Eddy *et al.* 2006). However, the best options involve recycling, reuse and resource recovery (Eddy *et al*. 2022). Re-use and recycling have been widely investigated and applied in the management of polymer waste but little has been achieved on resource recovery technology in the management of some solid wastes such as crustacean shells. Resource recovery embraces all approaches aim at deriving alternative resources from waste. Adsorption is a process that uses suitable materials (adsorbents) to remove or attract other materials (which may be toxic and undesirable) through a physical or chemical mechanism or both. Adsorption techniques have been successfully applied in the management of several environmental contaminants such as heavy metals, detergents, dyes, pharmaceuticals, etc. (Garg *et al*. 2021).

*Corresponding author, Ph.D.,
E-mail: okon.nnabuk@unn.edu.ng

The roles of nanomaterials in the improvement of existing technologies or the introduction of newer technologies have been widely attributed to their unique properties such as large surface area, optical properties, cost-effectiveness, and enhanced efficiency, among other factors (Eddy and Garg 2021). Toxic dyes have the potency of imparting severe consequences on the aquatic environment through the obscurity of light penetration (hence photosynthesis), the formation of non-biodegradable/stable products, termination of aquatic life, interference in water cycles, etc. (Odoemelam *et al*. 2018). Given their outstanding properties, the efficient removal of some environmental contaminants (such as dyes, heavy metals, antibiotics, industrial chemicals, etc.) from aqueous solution has been enhanced through the use of nanoparticles (Elaherif *et al*. 2021, Jalu *et al*. 2021).

Studies on the removal of toxic dyes are currently receiving severe research considerations because of the risk or burden that such contaminants can create for the future environment. Methyl orange is one of the known toxic dyes. It is commonly used in the textile and leather industries and tended to contaminate the environment and generate some toxicity symptoms such as vomiting and diarrhea at low concentrations and death at high concentrations (Aiseddig *et al*. 2017). The basic regulatory requirement for handling dye-contaminated water should therefore be centered on the

ISSN: 2287-237X (Print), 2287-2388 (Online)

removal of contaminants from aqueous solutions before disposal (Nasrollahzadeh *et al*. 2021). Among the steps that have been effectively investigated, adsorption is a well-known, highly efficient, effective and reproducible method (Garg *et al*. 2021). The application of the adsorption process in the remediation of the quality of the aquatic environment has been greatly enhanced by nanoparticles because of their advantages over their conventional counterparts (Das *et al*. 2018). Investigation into the application of calcium oxide nanoparticles (CaONP) is currently witnessing significant research interest since its composition is tolerable to the environment (Ramesh *et al*. 2017, Yoonus, *et al*. 2021). Therefore, the present study is aimed at synthesizing calcium oxide nanoparticles (CaONP) from periwinkle shells and the application of the synthesized CaONP for the removal of methyl orange dye from aqueous solutions through the batch adsorption process. The study shall provide solutions to resource recovery from solid wastes (which can affect the land and the water environment more severely) and the remediation of aquatic pollution by toxic dyes. Computational chemistry tools are also employed to support the experimental data.

2. Materials and methods

2.1 Preparation of the CaONP

The calcium oxide nanoparticles were prepared using the sol-gel method (Jalu *et al*. 2021). The precursor (periwinkle shells) were washed thoroughly with distilled water and dried in the oven at 100 °C for 24 hours. The dried samples, which are rich in $CaCO_3$ were crushed to a powder form and re-dried under the same condition. Sol-gel synthesis (see Eq.s below) was facilitated by the reaction of the precursor with HCl to form $CaCl_2$ (step 1) the calcium chloride produced was hydrolyzed to produce $Ca(OH)_2$ using NaOH (step 2) while the $Ca(OH)_2$ was calcined to CaONP at 900 °C. (step 3) The product was stored, characterized and used for the adsorption study.

$$CaCO_3 + 2HCl \rightarrow CaCl_2 + H_2O + CO_2 \text{ (step 1)}$$

$$CaCl_2 + 2NaOH \rightarrow Ca(OH)_2 + 2NaCl \text{ (step 2)}$$

$$Ca(OH)_2 \xrightarrow{900\ ^\circ C} CaO\ (nanoparticles) + H_2 \text{ (step 3)}$$

2.2 Characterization of the adsorbent (CaONP)

The mechanical property of the adsorbent was investigated using nanoindentation (Hysitron nanoindenter, Model T1950). The output data were used to plot loading-unloading graphs and the associated properties (such as hardness, depth of penetration, elastic modulus, power-law coefficients and others, were obtained after appropriate calculations.

All absorbance measurements were carried out using Shimadzu UV- Visible spectrophotometer (UV-180 series) while Agilent infrared spectrophotometer (Carry 630 FTIR spectrometer) was used for the FTIR analysis. BET-Nova 4200e. was employed for particle size analysis.

The CaONP were also characterized using XRD (Model PANalytical X'Pert Pro) using Cu–Kα radiation (K = 1.5406 A˚) operating at a voltage of 45 kV and 2Θ ranging from 20- 80º at a continuous speed of 0.045º per min. The thermal stability of the synthesized CaONP was analyzed using a thermogravimetric analyser. The wavelength of maximum absorption was obtained using an ultraviolet-visible spectrophotometer (UV7520-SEARCHTECH instrument). This wavelength served as the reference wavelength for all analyses involving the dye.

The transmission electron microscope (TEM) was obtained from Fei Tecnai G2 20 XT win equipment which has a tungsten cathode and operated under an acceleration voltage of 200 kV. The Scanning electron microscope (SEM) (Jeol JSM-6100) was also used to obtain the SEM image of the CaONP. The DLS experiment and zeta potential measurement were performed using a Zetasizer pro (Malvern Panalytical). The scanning was done to produce plots for size distribution by intensity and volume, correlogram, size quality report, cumulant and distribution fit reports.

2.3 Adsorption study

An adsorption study was performed as described earlier (Ekop and Eddy, 2010). The concentration of the dye before and after adsorption (i.e., C_o and C_e respectively) were used to calculate the percentage of dye adsorbed Eq. (1) and the equilibrium amount of the adsorbed dye Eq. (2) as follows:

$$\text{Percentage of dye adsorbed (\%)} = \left(\frac{C_o - C}{C_o}\right) \times 100 \quad (1)$$

$$Q_e(mg/g) = \left(\frac{C_o - C_e}{C_o}\right) \times \frac{V}{m} \quad (2)$$

where Q_e is the adsorption capacity of the adsorbate at equilibrium, V is the volume of the solution used for the adsorption experiment and m is the mass of the adsorbent. Concentrations of the methyl orange dye in the solutions were analyzed using a spectrophotometric method as described elsewhere (De Carvalho *et al*. 2015). A UV-visible spectrophotometer (UV7520-SEARCHTECH INSTRUMENT) was used to draw the calibration curve, which fitted perfectly and the concentration of all the test solutions was in turn calculated through extrapolation from the calibration curve (after the measurement of absorbance).

The effect of the initial concentration of the dye (using different concentrations of the dye), adsorbent dosage (using different masses of the adsorbent), period of contact (using different contact times), agitation speed (using different speeds of agitation), ionic strength (using 0.1 to 0.6 M NaCl) and temperature (at 30 to 70 °C) was investigated by the batch adsorption process. Except for the investigation of the effect of adsorbent dosage, the mass of the adsorbent used for all the experiments was 1 g.

2.4 Computational chemistry calculations

Computational chemistry calculations were carried out using ChemBio version 18 (for drawing of chemical structure), hyperchem release 10 (for calculation of binding/ adsorption energy) and Spartan for DFT calculations.

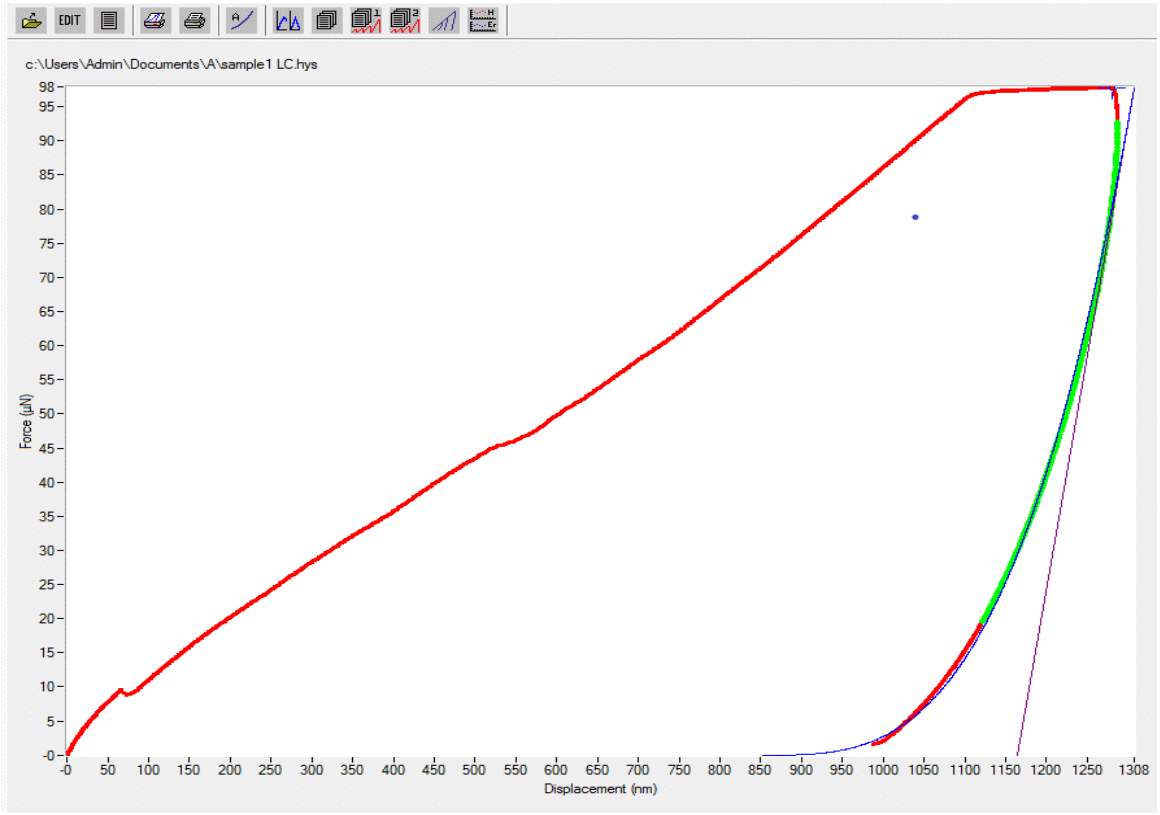

Fig. 1 Loading and unloading curves

Geometric optimization was carried out to obtain the most stable configuration before all calculations.

3. Results and discussion

3.1 Mechanical property: nanoindentation study

Nanoindentation was carried out to investigate the mechanical properties of the CaONP. Fig. 1 shows the loading and unloading curves for the CaONP. Mechanical parameters deduced from the plots were contact depth eq. (3), hardness Eq. (4) reduced elastic modulus Eq. (5) and contact stiffness Eq. (6):

$$h_c = h - \varepsilon \frac{P}{S} \tag{3}$$

$$H = \frac{P}{A} \tag{4}$$

$$E_r = \frac{S}{2}\sqrt{\frac{\pi}{A}} \tag{5}$$

$$S = 2E_r\alpha = 2\,tan(\theta)\,E_r h_c \tag{6}$$

where h is the indentation depth, ε is a constant, which is a function of the system geometry, P is the load $\left(P = \alpha(h - h_f)^m\right)$, which can also be defined in terms of the power law model, A is the contact area, S is the contact stiffness and E_r is the reduced elastic module which is a function of indentation depth (Qian and Zhao 2018).

The hardness, H is defined as the ratio of load to the projected contact area (A) between the indenter and the nanoparticles. It is a function of the indentation depth and contact area (Dhong *et al*. 2019). The measured indentation depth for the nanoparticle was 1200.2 nm while the contact area was 35290359.6 nm^2. The hardness under an applied force of 97.8 µN was 2.77 MPa which is relatively comparable to the value reported by Vahdat *et al*. (2020) for nanocomposite hydroxyapatite adsorbent. These properties are significant because a good adsorbent must have high mechanical strength among other properties. Also, the reduced elastic modulus of a material measures the resistance of that material to deformation. Jayakaran *et al*. (2019) stated that the modulus (120 MPa) and stiffness (1 TPa) of graphene are some of the factors that account for the effective removal of impurities from water. The reduced modulus of the synthesized CaONP is 101.77 MPa while the measured stiffness is 0.7 TPa, which is relatively comparable to that of graphene adsorbent. Calculated power-law coefficients for the CaONP included h_f = 3.179, m = 852.240 and α = 3.4 E 07. A young modulus value of 207.6 GPa has been reported for monolayer graphene oxide nanomaterials, which was acknowledged as an effective adsorbent for the removal of some pollutants from an aqueous solution (Soomro *et al*. 2012).

Values ranging from 39.7 to 76.8 MPa have also been reported for some pristine graphene. Other values in the range close to the value observed for CaONP have also been reported for some nanomaterials (Rahman *et al*. 2019, Suk *et al*. 2010).

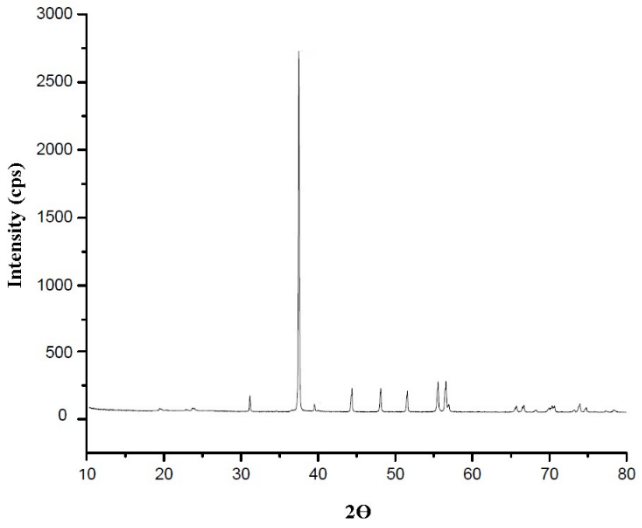

Fig. 2 XRD spectrum of the synthesized CaONP

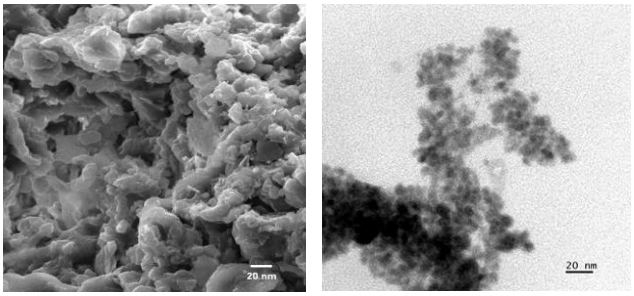

(a) (b)

Fig. 3 (a) SEM (b) TEM micrographs of the synthesized CaONP

Table 1 Frequency, intensity and associated functional of IR absorption by CaONP before and after the adsorption of methyl orange from aqueous solution

Before absorption		After absorption		Assignment
Wave number	Intensity	Wave number	Intensity	
-	-	404.01	92.397	Ca-O vibration
414.38	98.630	415.27	96.658	
422.05	98.690	426.83	96.288	
422.05	96.690	445.54	96.695	
-	-	461.91	97.121	
711.58	87.549	711.59	90.080	
870.52	78.367	872.16	84.398	Ca-O-Ca bond
1395.86	77.526	1403.40	86.279	C-O vibration
1795.50	98.554	1795.93	99.121	weak carbonate C=O bond
-	-	2372.52	99.131	

3.2 X-ray diffraction (XRD) spectroscopy

XRD analysis was used to characterize the crystalline phase and purity of the nano-adsorbent. The XRD pattern of CaONP is shown in Fig 2, along with its distinctive peaks. The diffraction patterns clearly show that the CaONP displays characteristic peaks for CaO at 2θ equal to 32.3°, 37.1°, 44.2°, 48.5°, 52.4°, 55.8°, and 57.2°. The narrow and intense peak at 2Θ= 37.1° in the patterns can be accredited to the crystalline nature of nano-CaO (Jalu *et al*. 2021b). This distinctive, narrow, and strong peak was assigned to the 104 planes and attributed to the calcite phase. Additionally, the XRD pattern revealed no peak associated with any other component, confirming the product's purity.

3.3 Scanning (SEM) and Transmission (TEM) electron microscopy

As seen in Fig. 3a, the SEM image of the CaONP reveals that the CaONP presents a flake-shaped morphology with some porous nature and a tendency towards agglomeration. The dimensions of the nanoparticles were evaluated by using image J-software and the results obtained indicated the particle size to have an average value of 17 nm. Also, the TEM image in Fig. 3b reveals flake-like particles with some tendency toward aggregation. The average particle size obtained from the TEM was 20 nm. Consequently, the CaONP is a mesoporous material.

3.4 Fourier transformed infra-red (FTIR) analysis

The FTIR spectrum of the CaONP synthesized from the periwinkle shells is shown in Fig.4a. The disappearance of an absorption band due to trioxocarbonate (IV) reveals that there was a complete conversion of $CaCO_3$ to CaO. Typical frequencies for the FTIR spectrum of $CaCO_3$ are a broad absorption band at 1420-1480 cm-^{1} and a sharp peak at 872 cm^{-1} (Garg, Kumari, *et al*. 2021). However, there was no observable peak at 1420-1480 cm^{-1} and a weak peak at 872 cm^{-1} which suggests that almost all the $CaCO_3$ was converted to CaO. This peak (872 cm^{-1}) has also been linked to Ca-O-Ca vibration by (Maringgal *et al*. 2020) which may not be due to the presence of $CaCO_3$. The peak at 712 cm^{-1} is due to CaO vibration (Ramli *et al*. 2019). The FTIR spectrum of the methyl orange dye (Fig. 4b) indicated the presence of OH stretching at 3267 and 2925 cm^{-1}, C=O stretching at 1738 cm^{-1}, C=C stretching at 1606 cm^{-1}, N-O stretching at 1520 cm^{-1}, S-O stretching at 1418 cm$^{-1,}$ C-N stretching at 1237 cm^{-1} and CH_2 wagging at 1011 cm^{-1} (Wu *et al*. 2021). After the adsorption of the methyl orange dye by CaONP, the resulting FTIR spectrum (Fig. 4c) reveals the presence of several CaO vibrations at various frequencies in addition to Ca-O-Ca vibration and a very weak carbonate C=O bond (Table 1).

3.5 Thermogravimetric/differential thermogravimetric analyses (TGA/DTA) and BET analyses

The TGA and DTA plots of the CaONP are shown in Fig. 5a. The first peak was observed between 100 and 160 °C which corresponds to a loss of adsorbed water. Between 270 and 317 °C, the observed peak corresponded to a mass loss of about 23 % while 44 % mass loss aligned with a temperature range of 442 and 550 °C. This may be attributed to the decomposition of some adsorbed organic matter. Within the temperature range of the TGA analysis, the final loss in mass started at 550 °C.

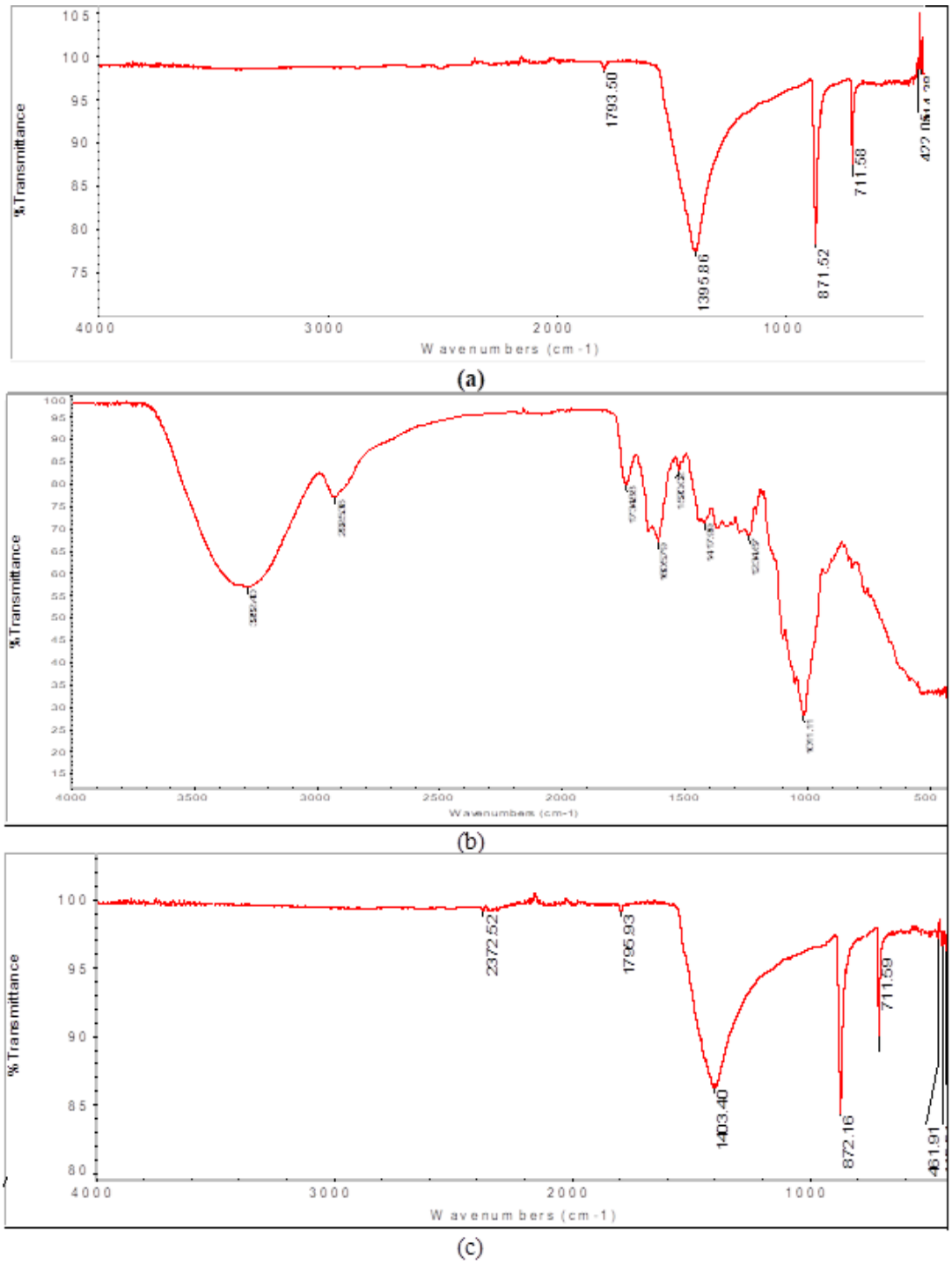

Fig. 4 FTIR spectrum of (a) CaONP (b) methyl orange dye (c) CaONP after adsorption

It suffices to state that for the adsorption study, the synthesized CaONP is stable within the temperature range employed for the adsorption study. The close similarity in the observed TGA trend has been reported by (Mirghiasi *et al*. 2014) for CaONP synthesized through high temperature calcination of $Ca(OH)_2$. The DTA plot shows a major endothermic dip at about 400 °C, which may be due to the crystalline transformation of the CaONP. A similar dip was observed by (Ashok *et al*. 2015). Other DTA peaks occurred around 100 and 650 °C.

The nitrogen adsorption isotherm for CaONP according to BET analysis is shown in Fig. 5b. The plot reveals an excellent fitness and from BET measurement, pore properties of the synthesized CaONP were BET surface area = 138.998 m^2/g, pore diameter = 2.92 nm and pore volume = 1.668 ccc/g. These values place the synthesized CaONP as mesoporous materials which are unique for the efficient adsorption process. The BET analysis seems to show better pore size evaluation because the DLS method depends on the nature of the dispersant used and other parameters that

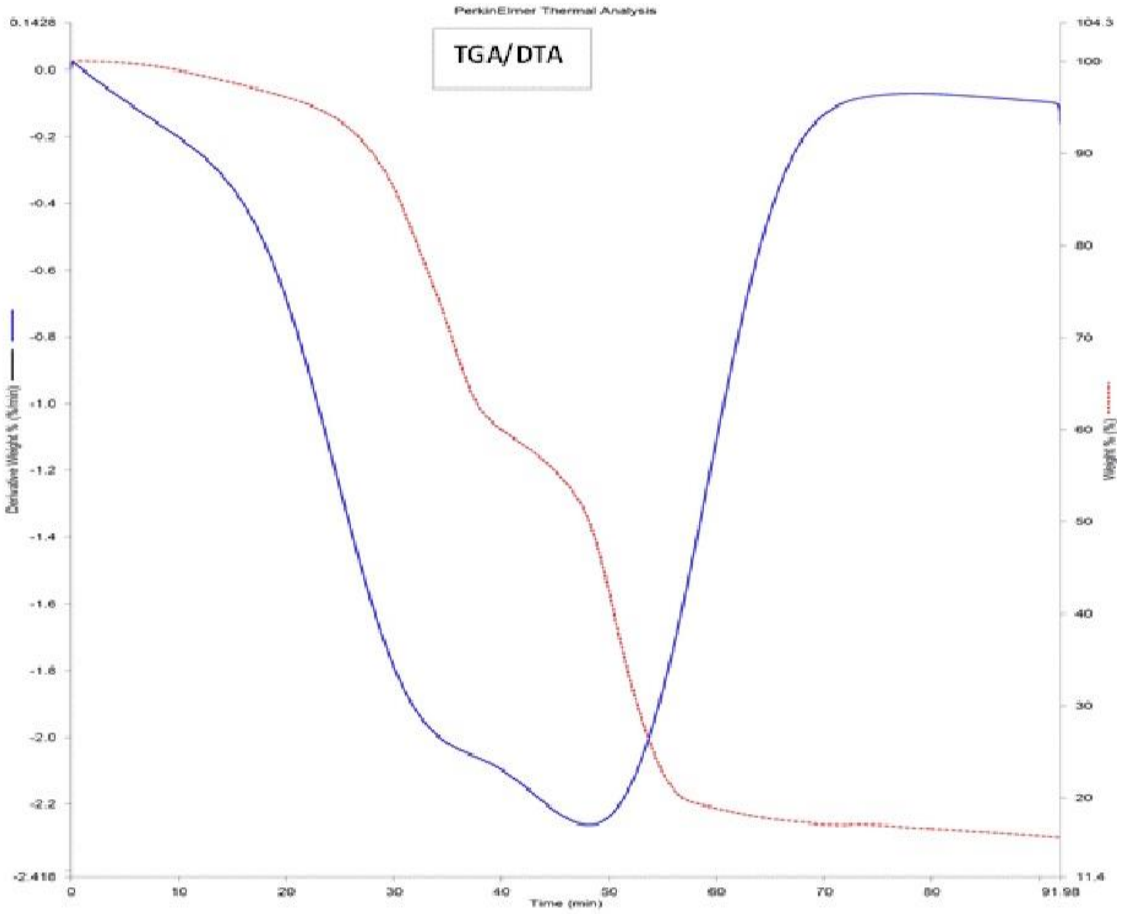

(a)

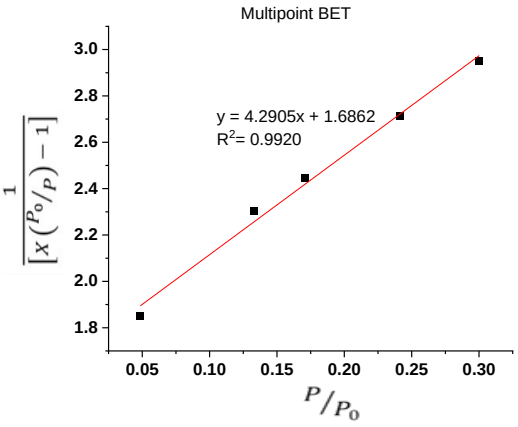

(b)

Fig. 5 (a) TGA/DTA of the CaONP synthesized from periwinkle shell (b) BET isotherm for N2 adsorption by CaONP

can be altered. Fig. 6 shows the dynamic light scattering plots for CaONP consisting of (a) particle size distribution by volume and (b) particle size distribution by number. Based on size distribution by volume, 0.7% of the volume is occupied by nanoparticles with an average diameter of 54.90 nm) while 90.3% consisted of those with an average diameter of 10 nm (100% size distribution by number). However the average diameter of 9.83 nm was observed based on distribution by number. Consequently, the synthesized nanoparticles lie in the mesoporous range, which is comparable to the average size obtained from TEM analysis.

3.6 Batch adsorption study

Fig. 6 shows the variation of the equilibrium amount of dye adsorbed with pH and the Zeta potential plot for the CaONP. The consideration of the trend observed for the two

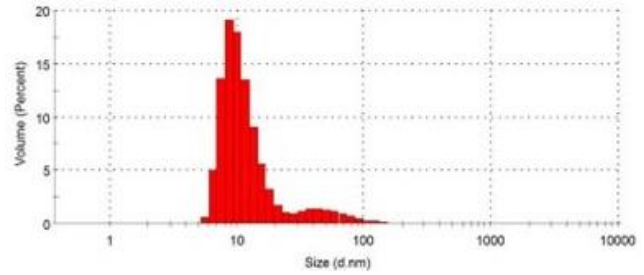

(a)

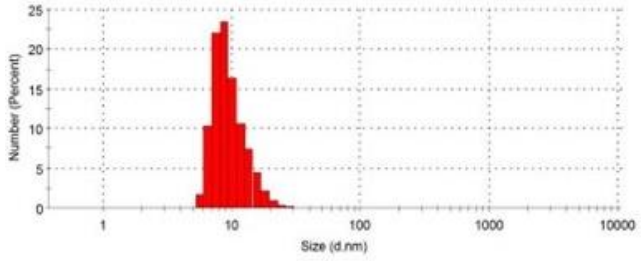

(b)

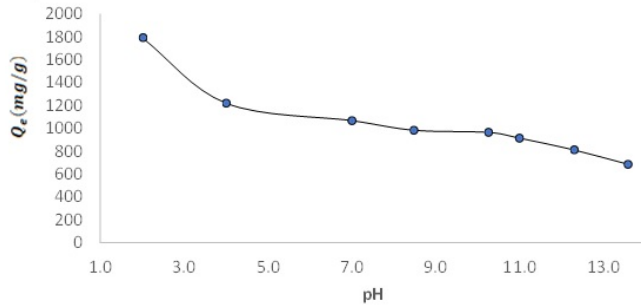

(c)

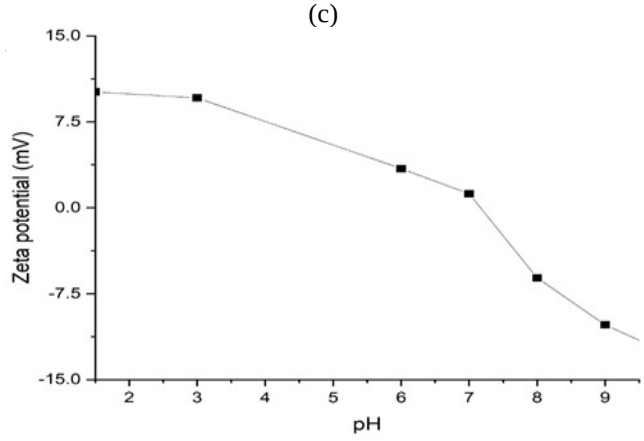

(d)

Fig. 6 (a) particle size distribution by volume and (b) particle size distribution by number (c) Variation of Q_e and (d) and Zeta potential

plots confirms that the adsorption of the dye is favoured by acidic pH. Fig 7a is a plot showing the variation of the amount of methyl orange dye adsorbed at equilibrium with the initial concentration of the dye. The plot reveals a typical feature expected for linear adsorption because the equilibrium concentration of the adsorbed dye increases proportionally with an increasing initial concentration of the dye. This observation signifies the progressive absorption of the dye molecules on the available active sites of the nanoparticles as diffusion increases. Nanomaterials are known for their large activated surface area, which favors adsorption (Nasrollahzadeh *et al*. 2021). Although literature reports good adsorption efficiencies of periwinkle, oyster and snail shells for some contaminants, it is obvious from the present study that the CaONP showed better efficiency than any of the crustacean shells (Odoemelam and Eddy, 2009). Generally, an increase in diffusion will lead to an enhancement in adsorption, provided the number of active adsorption sites is not exceeded.

The results obtained by variation of contact time indicated an initial rise in the adsorption of methyl orange dye (Fig. 7b).

The initial adsorption rate was 0.4 mg/min (after 10 min of contact between the adsorbate and the adsorbent) then progresses after 40 minutes (where the adsorption rate increased to about 0.7 mg/min) and finally became steady. The trend is a direct explanation of the tendency of the initial adsorption to increase owing to the availability of sufficient numbers of active adsorption sites along with the dominated forces of adsorption (at this stage) over the forces of desorption (Odoemelam *et al*. 2018). At equilibrium (which started after 40 min of contact), the two forces were balanced and a steady-state (defining equilibrium between adsorption and desorption) was observed. A similar trend has been observed by others. For example, Yunusa *et al*. (2021) attributed such to the magnitude of the driving force between the concentration gradient (which is dependent on the rate of diffusion of the dye molecules) and available adsorption sites. Adsorption can be influenced by factors associated with agitation such as the method of agitation, speed of agitation, etc. Fig. 7c also contains a plot depicting the effect of different agitation speed on the adsorption of methyl orange dye.The plot reveals that the dye adsorption increases with an increase in the speed of agitation. An increase in the speed of agitation from 100 to 500 rpm led to an increase in the adsorption peak up to 99.98 %.

Kuśmierek and Świątkowski (2015) reported similar findings and attributed the observation to a corresponding increase in the rate of diffusion of the adsorbate molecules towards the liquid boundary layer from the bulk liquid. Agitation improves fragmentation of the adsorbent layer adsorption through its tendency to increase turbulence and fragmentation of the adsorbent molecules as well as decrease the thickness of the liquid boundary layer (Miyah *et al*. 2017). The adsorption of methyl orange dye on the surface of CaONP was also observed to decrease with an increase in temperature (Fig.7d), indicating that the adsorption of the dye from the aqueous solution conforms with the mechanism of physical adsorption in consistence with other reported results (Lafi *et al*. 2020, Mekatel *et al*. 2015). The ionic strength of a solution can affect the adsorption of a dye such as methyl orange in one of the following ways: (i) the enhancement of adsorption (synergism), (ii) the enhancement of desorption (antagonism) and (iii) absence of antagonism and synergism (Lafi *et al*. 2020). The influence of ionic strength on the removal of methyl orange from aqueous solution by CaONP was also investigated and the obtained results (Fig. 7e) indicated enhanced adsorption with an increase in ionic strength of

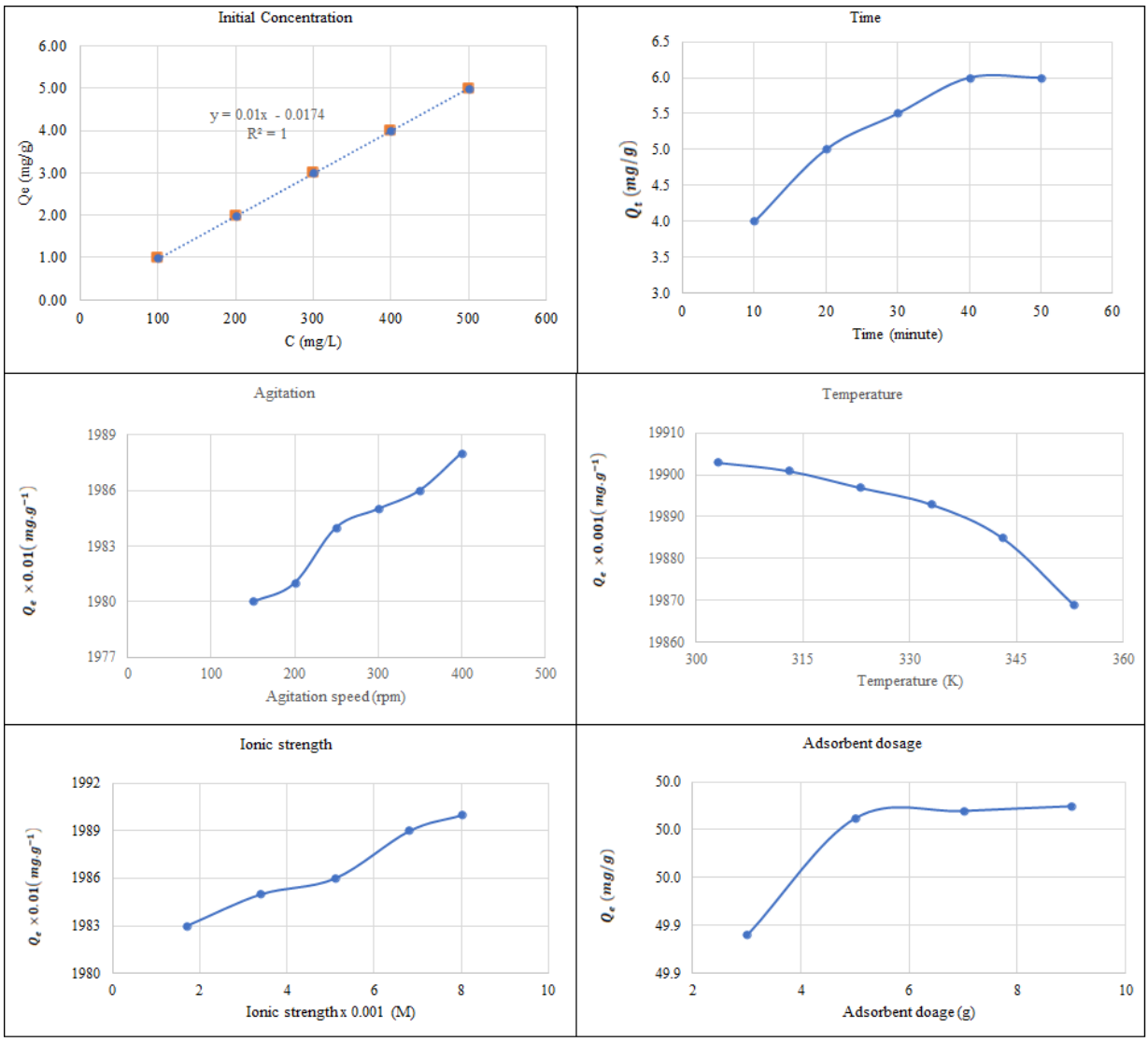

Fig. 7 Variation of equilibrium amount of methyl orange dye adsorbed by CaONP with (a) initial concentration (b) time (c) agitation speed (d) temperature (e) ionic strength and (f) adsorbent dosage

the solution. This is due to the enhancement of the adsorption by a synergistic combination of the dye and the NaCl. A similar observation reported by Al-Degs *et al*. (2008) for the enhancement of the adsorption of some reactive dyes onto activated charcoal was attributed to enhanced adsorption that arose from an increase in the aggregation of the dye molecules in the solution. Benaïssa, (2010) also reported that the extent of adsorption removal of methyl orange from an aqueous solution (by almond peel) increases with increasing concentration of NaCl in the solution.

Other reported findings that agree with the present result on the influence of ionic strength are those reported by (Boumediene *et al*. 2018) for the removal of methylene blue by orange peel and the work of (Lafi *et al*. 2020) for the removal of methyl orange from aqueous solution by modified extracted cellulose. The amount of methyl orange dye adsorbed by CaONP varied with adsorbent dosage. A sharp rise in the adsorption process was observed as the adsorbent dosage increases from 1 to 6 g before an equilibrium state was established (I.E, above this dosage). An increase in adsorbent dosage can increase the number of available and active adsorption sites as reflected in the first section of the plot (Fig. 7f). However, when all the active molecules that diffused to the adsorption sites were completely adsorbed, an equilibrium was established (De Carvalho *et al*. 2015). A deviation from the equilibrium can either lead to desorption causing a decline in the amount of adsorbed dye or a further increase (if more activated adsorption sites are energized). In this study, a shift in equilibrium was not observed even at an adsorption dosage of 6 g. A similar trend has been reported for the adsorption of methyl orange dye by other nano and non-nano adsorbents (Mekatel *et al*. 2015, Wu *et al*. 2021).

3.7 Study of the Kinetics

The models defining the pseudo second order kinetics and intraparticle diffusion model given by Webber-Morris were tested for their fitness in the explanation of the

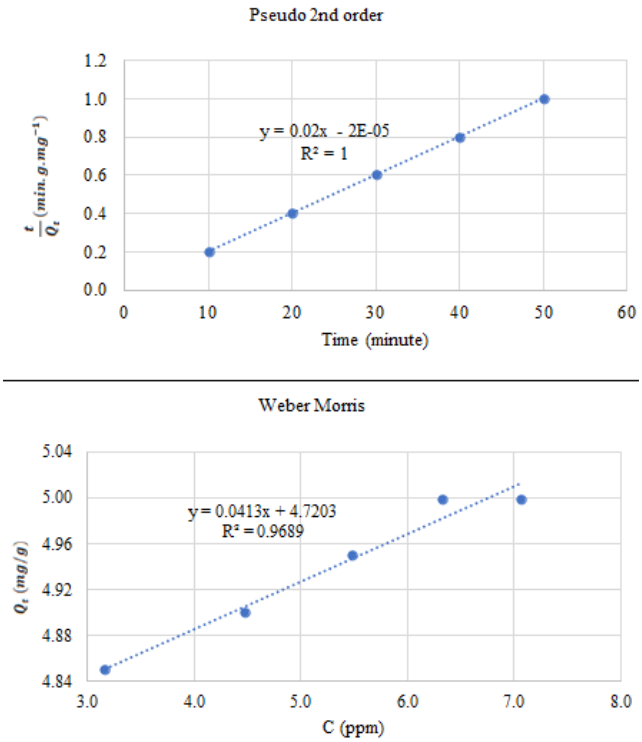

Fig. 8 Pseudo second order and Weber Morris kinetic plots for the adsorption of methyl orange dye on CaONP

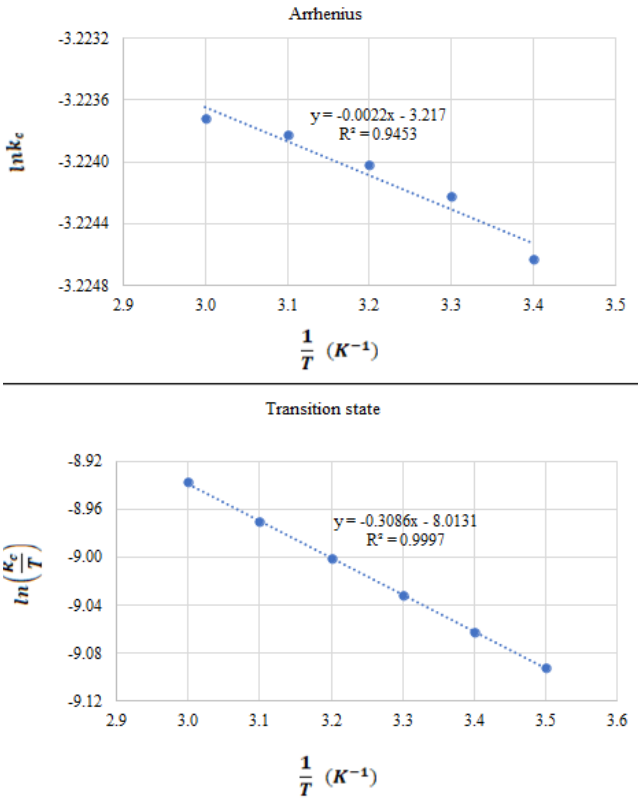

Fig. 9 Arrhenius and Transition state plots for the adsorption of methyl orange dye on CaONP

adsorption of methyl orange by the synthesized CaONP (Miyah *et al*. 2017). The kinetics data obtained for the adsorption of methyl orange unto CaONP fitted the pseudo second-order kinetics (Eqs. 7 to 10) perfectly (R^2 = 1). (Miyah *et al*. 2017) as follows:

$$Q_t(1 + k_2 Q_e t) = k_2 Q_e^2 t \quad (7)$$

$$(k_2 Q_e^2 t)/Q_t = 1 + k_2 Q_e t \quad (8)$$

$$\frac{(k_2 Q_e t)}{k_2 Q_e^2 Q_t} = \frac{1}{(k_2 Q_e^2)} + \frac{k_2 Q_e t}{k_2 Q_e^2} \quad (9)$$

$$\frac{t}{Q_t} = \frac{1}{k_2 Q_e^2} + \frac{t}{Q_e} \quad (10)$$

The theoretical equilibrium amount of adsorbed dye as obtained from the pseudo second-order plot (Fig. 8) is 0.6 while the pseudo-second-order rate constant (k_2) is 200 g.mg min^{-1}. Also, the theoretical value of the initial adsorption rate, which is proportional to the square of Q_e (i.e. $h_0 = k_2 Q_e^2$), was estimated as h_0 = 5.00. This value is very close to the experimentally determined value of 4.9873 mg/g.

The intraparticle diffusion model proposes that the uptake of the adsorbate is proportional to the square root of the period of contact as shown in Eq. 11 (Jasper *et al*. 2020):

$$Q_t = k_{id}\sqrt{t} + C \quad (11)$$

where k_{id} is the intraparticle diffusion constant (in $mg.g^{-1}min^{-1}$).

A linear plot was obtained for the variation of Q_t with $\sqrt{t}$ (graph not shown) and the slope gave k_{id} to be equal to 0.0413 therefore, the diffusion of methyl orange molecules to the surface of CaONP has dominant control over the adsorption.

3.8 Thermodynamic study

The equilibrium constant for the adsorption process was calculated as the ratio of the concentration of the dye at equilibrium to the initial concentration of the dye i.e. $k_c = \frac{C_e}{C_o}$ (Senthil Kumar *et al*. 2014). The relationship between the equilibrium constant and the standard free energy of adsorption Eq. (12) was further explored to compute the associated thermodynamic parameters Eq. (13)-(15):

$$\Delta G_{ads}{}^{o} = -RTlnk_C \quad (12)$$

$$\Delta G_{ads}{}^{o} = \Delta H - T\Delta S \quad (13)$$

$$-RTlnk_C = \Delta H - T\Delta S \quad (14)$$

$$ln\, k_c = \frac{\Delta S}{R} - \frac{\Delta H}{RT} \quad (15)$$

Eq. (15 represent a linear model that implies a plot of $ln\, k_c$ versus $\frac{1}{T}$ (Fig. 9) with a slope equal to $-\frac{\Delta H}{R}$ and intercept equal to $\frac{\Delta S}{R}$. Average enthalpy and enthalpy changes deduced from the plot are -2.57 and -66.63 J respectively. Therefore, the adsorption of the methyl orange dye is endothermic and ordered (Yunusa *et al*. 2021).

The activation energy was also estimated through the application of the Arrhenius Eq. (16) (Ahmad *et al*. 2014):

$$ln\, k_c = ln\, A - \frac{E_a}{RT} \quad (16)$$

Therefore, a plot of lnk_c versus 1/T was linear (Fig. 9) and the estimated activation energy was 0.018291 J/mol, which lies in the range of values typically accounting for physisorption.

3.9 Adsorption isotherm

Adsorption isotherm is significant because it can provide information on the adsorption characteristics of the adsorbate (Miyah *et al*. 2017). Some of the established isotherms are Langmuir, Freundlich, Temkin, Flory-Huggins, Frumkin, etc. Experimental data was tested o obtain the best-fit isotherm and the test reveal that the adsorption characteristics of methyl orange dye are best explained by Langmuir adsorption isotherm. The Langmuir isotherm applies to monolayer adsorption on a homogeneous surface with a finite number of adsorption sites and without any interaction between the adsorbed molecules (Ekop and Eddy 2010). The corresponding expression is given by Eq. (17) (Mehr *et al*. 2019):

$$Q_e = \frac{Qe_{max}}{1 + bC_e} \quad (17)$$

where Q_{max} denotes the maximum adsorption capacity of the adsorbent and b, the Langmuir constant is related to the heat of adsorption. Eq. (17) can be simplified into various linear forms as follows:

$$\frac{C_e}{Q_e} = \frac{1}{Q_{max}\frac{C_e}{Q_{max}}} \quad (18)$$

$$\frac{1}{Q_e} = \frac{1}{Q_{max}\frac{1}{C_e}\frac{1}{Q_{max}}} \quad (19)$$

$$Q_e = Q\frac{1}{b}\left(\frac{Q_e}{C_e}\right)_{max} \quad (20)$$

$$\left(\frac{Q_e}{C_e}\right) = bQe_{max} \quad (21)$$

Based on Eq. (19), the plot of $\frac{1}{Q_e}$ versus $\frac{1}{C_e}$ was linear for the adsorption of methyl orange dye onto CaONP as evident in Fig. 10. The adsorption parameters derived from the plots have been listed in Table 2. Generally, the Langmuir is otherm is ideal for monolayer adsorption on a homogenous surface that has a finite number of adsorption sites and where there is no interaction between the adsorbed molecule (Mehr *et al*. 2019).

Significant information on the favorability of the adsorption process through the binding constant deduced from the Langmuir isotherm using the Eq. (Miyah *et al*. 2017):

$$R_L = \frac{1}{1 + bC_o} \quad (21)$$

R_L values less than unity suggest favorable adsorption while those that are greater than unity are consequences of unfavorable adsorption. Hence, the adsorption of methyl orange on the surfaces of CaONP is favorable at all concentrations because R_L values are less than unity (values not shown). Also, the Langmuir equilibrium constant of adsorption, b can be deduced from the change in standard free energy change, $\Delta G_{ads}{}^{o}$ according to Eq. 23:

$$\Delta G_{ads}{}^{o} = -RTln(b) \quad (23)$$

The calculated free energy is negative and is within the limit expected for the mechanism of charged transfer reflecting the adsorption of the dye as spontaneous and effectively occurring through the physisorption mechanism (Lafi *et al*. 2020).

The Temkin adsorption isotherm is useful for the explanation of the interaction between the adsorbent and the adsorbate. The isotherm operates on the assumption that at moderate concentration, the heat of adsorption will decrease linearly with the surface coverage. The linear form of the isotherm is as expressed by Eq. 24 (Mekatel *et al*. 2015):

$$Q_e = B\, ln\, A_T + B\, ln\, C_e \quad (24)$$

where A_T (L/g) and B (J/mol) are the Temkin constants which represent the binding equilibrium isotherm and the heat of adsorption respectively. The adsorption of methyl orange dye by CaONP obeyed the Temkin adsorption model with high linearity (R^2 = 0.9473 and 0.9497) evident in Fig. 10 with the deduced Temkin adsorption parameters recorded in Table 2. The Temkin constant, B is related to the heat of adsorption while A_T is the empirical constant that is related to the equilibrium binding constant and hence the maximum binding energy (L/mg) (Ahmad *et al*. 2014).

Table 2 Langmuir and Temkin parameters for the adsorption of methyl orange on CaONP

Langmuir parameters		Temkin parameters	
Slope	103.16	Slope	2.4239
Q_{max}	156.25	Intercept	10.498
b	6.204 E -05	lnA_T	4.331
ΔG^0_{ads} (kJ/mol)	-24.409	B	2.4239
R^2	1.000	R^2	0.9473

3.10 Computational chemistry study: Global reactivities (molecular mechanics and semiempirical parameters)

The optimized structure of methyl orange dye is shown ahead. The molecule contains two benzene rings that are separated by two imine nitrogen. One end of the aromatic ring ends with sulphone while the other end with the enamine nitrogen group. The compound is rich with heteroatoms (S, O, N) and has electropositive sodium attached to the sulphone group. Therefore, its adsorption capacity may be significant on surfaces such as CaONP. Initial molecular mechanics calculations performed on the bulk molecules indicated four lone pair electrons associated with two oxygen atoms in the sulphone end and two others (one to each of the imine nitrogen) in the center of the molecule. The methyl orange molecule can be viewed as a

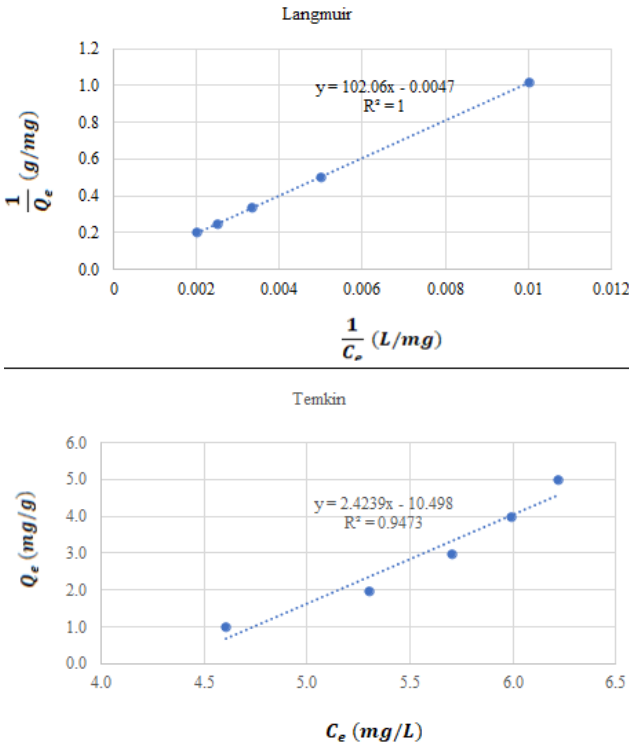

Fig. 10 Temkin and Langmuir plots for the adsorption of methyl orange on CaONP

Table 3 Molecular mechanics parameters for methyl orange dye and its moieties

Parameters	Methylene orange	Benzo-sulphone	Benzo-emanine
Stretch	1.7351	1.0652	0.8446
Bend	141.9393	148.3554	8.2099
Stretch-Bend	-0.1094	-0.9075	0.3735
Torsion	27.7835	26.0904	-7.7043
Non-1,4 VDW	2.1987	12.6160	3.7613
1,4 VDW	20.5491	8.6961	11.4497
Charge/Charge	-18.4750	-109.2459	-
Charge/Dipole	-5.8266	-12.9273	-
Dipole/Dipole	14.4275	15.3695	0.0101
Total Energy (kcal/mol)	184.223	89.119	16.9448

combination of two benzene rings having their sulphone and enamine ends bridge together by the two imine nitrogen atoms (Fig. 11). MM2 energy minimization for the methyl orange dye and the benzo-enamine and benzo-sulphone moieties gave results shown in Table 3. The total energy of the dye is greater than the sum of the energies from the two moieties, which implies that additional energy of interaction caused by the bridging of the two imine nitrogen atoms may be responsible for the maintenance of the compound. Bending stretch, torsion and dipole-dipole interactions are lower for the enamine moiety. The absence of free charge seems to make charge-charge (i.e., ion-ion) dipole and charge-dipole (i.e. ion-dipole) interactions to be absent in benzo enamine but stronger in the benzo sulphone moiety.

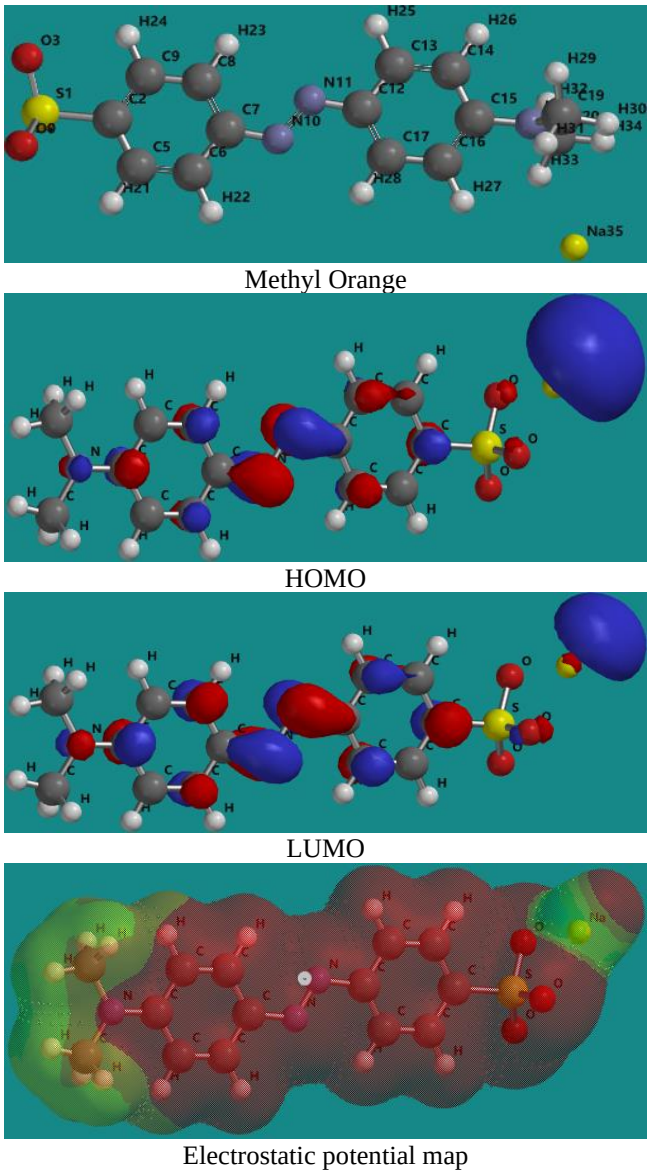

Fig. 11 Variation of equilibrium amount of methyl orange dye adsorbed by CaONP with initial concentration, time, agitation speed, temperature, ionic strength and adsorbent dosage

The usefulness of the frontier molecular orbitals energies in adsorption is significant because adsorption involves the transfer of charge or electrons. Consequently, the highest occupied molecular energy (E_{HOMO}) is an index for the measurement of the tendency towards the donation of electrons or charge while the lowest molecular orbital energy (E_{LUMO}) measures the tendency toward the acceptance of electrons (Eddy and Ameh 2021). The energy gap is reflected by the difference, $E_{LUMO} - E_{HOMO}$, which is a measure of the proximity toward electron transfer from the HOMO to the LUMO (Ameh and Eddy 2018).

The adsorption of methyl orange dye onto the surface of CaONP has been shown to proceed through the physisorption mechanism indicating that charge transfer from the charge dye molecule to the charge adsorbent surface is an essential step in the adsorption process. The

Table 4 Molecular mechanics parameters for methyl orange dye and its moieties

Atom (No)	Electrophilic (f_x^-)		Nucleophilic (f_x^+)		Radical (f_x^0)	
	Mulliken	Hirshfeld	Mulliken	Hirshfeld	Mulliken	Hirshfeld
C(1)	0.005	0.033	0.028	0.046	0.016	0.039
C(2)	0.010	0.025	0.015	0.031	0.013	0.028
C(3)	0.001	0.027	0.023	0.037	0.012	0.032
C(4)	0.031	0.013	0.003	0.017	0.017	0.015
C(5)	0.009	0.020	0.032	0.034	0.020	0.027
C(6)	0.012	0.024	0.012	0.029	0.012	0.027
S(7)	0.004	0.009	0.007	0.012	0.006	0.011
O(8)	0.019	0.018	0.020	0.020	0.020	0.019
O(9)	0.030	0.030	0.033	0.034	0.031	0.032
O(10)	0.018	0.025	0.026	0.022	0.022	0.024
N(11)	0.129	0.105	0.074	0.083	0.101	0.094
N(12)	0.128	0.089	0.082	0.092	0.105	0.090
C(13)	0.038	0.036	-0.001	0.015	0.018	0.025
C(14)	-0.000	0.027	0.022	0.035	0.011	0.031
C(15)	0.009	0.037	0.011	0.028	0.010	0.033
C(16)	0.008	0.027	0.035	0.040	0.022	0.033
C(17)	0.010	0.035	0.012	0.031	0.011	0.033
C(18)	0.011	0.024	0.036	0.039	0.023	0.031
N(19)	-0.003	0.053	0.016	0.035	0.007	0.044
C(20)	-0.024	0.017	-0.023	0.013	-0.023	0.015
C(21)	-0.024	0.017	-0.022	0.013	-0.023	0.015
Na(36)	0.029	0.020	0.031	0.023	0.030	0.021

feasibility of the charge transfer process is significantly dependent on the frontier molecular orbital energies. The frontier molecular energies for the dye were E_{HOMO} = -6.19 eV, E_{LUMO} = -3.02 eV and ΔE = 3.17 eV. These values are consistence with the earlier reported values for some dyes that have been reportedly removed from an aqueous solution. For example, (Odoemelam *et al*. 2018) reported the E_{HOMO} for malachite green and methylene blue dyes as -5.6856 and -8.4071 eV respectively while their corresponding values of E_{LUMO} were -1.43227 and -2.604 eV. The evaluated energy gaps were 6.9743 and 3.0448 eV respectively. The removal efficiency of these dyes was strongly dependent on their frontier molecular energies which suggests that the values obtained for the studies methyl orange are probably more favorable for the adsorption process. The computational data for methyl orange dye obtained in this study, are also comparable to those reported for cationic dyes (Yunusa *et al*. 2021).

The HOMO and LUMO diagrams of methyl orange dye are shown in Fig. 11 revealing that the adsorption of the dye unto the CaONP occurs at the imine nitrogen bond, which seems to be the center for electron density arising from the two oppositely arranged benzene rings. The calculated dipole parameters of the adsorbate molecule are 59.17 D while its polarizability is 64.37. The values are comparable to those reported for the adsorption of methyl orange dye by other adsorbents (Junejo *et al*. 2021). The electrostatic potential map of methyl orange dye (also shown in Fig. 11) reveals the accessible surface area for the methyl orange dye to be 231.77 out of 336.88 Å^2 while the accessible volume was 310.98 Å^3. The accessible surfaces of the molecule (68 %) are indicated with a light red color in the figure. The electrostatic potential map shows three different sessions indicated with light red, light green and green colors, which correspond to highly receptive, less receptive and non-reactive sites respectively. The information shown by the electrostatic map, reveals some similarities with the HOMO and LUMO diagrams for this compound.

The condensed Fukui functions for electrophilic (Eq. 24), nucleophilic (Eq. 25) and radical (Eq. 26) attacks were used to evaluate the atoms/bonds for the respective attacks (Eddy and Ameh 2021). The Mulliken and Hiersfield charges were used for the calculations

$$f_x^+ = q_{(N+1)} - q_N \tag{25}$$

$$f_x^- = q_N - q_{(N-1)} \tag{26}$$

$$f_x^0 = \frac{\left(q_{(N+1)} - q_{(N-1)}\right)}{2} \tag{27}$$

Estimated Fukui indices are presented in Table 4. The results from both Mulliken and Hiersfield charges agree and indicated that the sites for electrophilic attack (which correspond to the site with the highest value of f_x^-), nucleophilic attack (corresponding to the site with the highest value off_x^+) and radical attacks (i.e. the site with the highest f_x^0 value) all reside in the imine nitrogen bond (i.e., N (11)-N(12) bond). The observed location aligns with the findings deduced from the electrostatic potential map and the diagrams for the HOMO and LUMO.

Therefore, in the adsorption of methylene dye unto CaONP surface, the activated charge surface will likely hold the dye at N(11)-N(12) position, each of which has a lone pair of electrons and is surrounded by an electron-rich aromatic ring that can present greater bond susceptibility towards reactivity.

The binding energy between the adsorbate and the adsorbent was evaluated using the following Eq. (Eddy and Ameh 2021):

$$E_{Bind(Adsorbate-CaONP)} = E_{Bind(T)} - \left(E_{Bind(CaONP)} + E_{Bind(Adsorbate)}\right) \tag{28}$$

where $E_{Bind(Adsorbate-CaONP)}$ is the binding energy between the adsorbate and the adsorbent, $E_{Bind(T)}$ is the total binding energy when both are together, $E_{Bind(CaONP)} + E_{Bind(Adsorbate)}$ are the respective binding energy of the adsorbent and the adsorbate. The calculated $E_{Bind(Adsorbate-CaONP)}$ (32. 9136 MeV) is within the expected range for the mechanism of physical adsorption (i.e. 10 to 300 MeV).

4. Conclusions

Periwinkle shell has a high concentration of $CaCO_3$ that can constitute a major precursor for the synthesis of calcium oxide nanoparticles. The characteristics of the synthesized

product have nano properties such as dimension, surface area and functional groups that support its application as an adsorbent for the removal of methyl orange dye from contaminated water. The kinetics study signified the role of diffusion of methyl orange dye towards the surface of CaONP. The removal capacity of the CaONP for the dye was found to be excellent and favors the physisorption mechanism. The adsorption was found to be endothermic and spontaneous. The imine functional groups are more useful for the removal because its provided adsorption sites for the adsorbate to interact effectively with the adsorbent. The physical adsorption of methyl orange by CaONP was also verified by their binding energy signifying the application of CaONP as an effective nano-adsorbent.

Acknowledgement

The authors greatly acknowledge the Tertiary Education Trust Fund of Nigeria for providing the National Research Fund grant for the project that generated this research under Prof. Nnabuk Okon Eddy as the Principal Investigator.

References

Ahmad, M.A., Ahmad Puad, N.A. and Bello, O.S. (2014), "Kinetic, equilibrium and thermodynamic studies of synthetic dye removal using pomegranate peel activated carbon prepared by microwave-induced KOH activation", *Water Resour. Ind.*, **6**, 18-35. https://doi.org/10.1016/j.wri.2014.06.002.

Al-Degs, Y.S., El-Barghouthi, M.I., El-Sheikh, A.H. and Walker, G.M. (2008), "Effect of solution pH, ionic strength, and temperature on adsorption behavior of reactive dyes on activated carbon", *Dye. Pigment.*, **77**(1), 16-23. https://doi.org/10.1016/j.dyepig.2007.03.001.

Ameh, P.O. and Eddy, N.O. (2018), "Experimental and computational chemistry studies on the inhibition efficiency of phthalic acid (PHA) for the corrosion of aluminum in hydrochloric and tetraoxosulphate (VI) acids", *Prot. Met. Phys. Chem. Surf.*, **54**(6), 1169-1181. https://doi.org/10.1134/S2070205118060035

Ashok, C., Chakra, C.S., Dayakar, T., Kumar, M.K. and Rao, K.V. (2015), "Calcium oxide nano particles synthesized from chicken egg shells by physical method calcium oxide nano particles synthesized from chicken egg shells by physical method", *Int. Conf. Emerg. Technol. Mech. Sci.*, 72-75.

Benaïssa, H. (2010), "Influence of ionic strength on methylene blue removal by sorption from synthetic aqueous solution using almond peel as a sorbent material: experimental and modelling studies", *J. Taibah Univ. Sci.*, **4**(1), 31-38. https://doi.org/10.1016/s1658-3655(12)60024-7.

Boumediene, M., Benaïssa, H., George, B., Molina, S. and Merlin, A. (2018), "Effects of pH and ionic strength on methylene blue removal from synthetic aqueous solutions by sorption onto orange peel and desorption study", *J. Mater. Environ. Sci.*, **9**(6), 1700-1711. https://doi.org/10.26872/jmes.2018.9.6.190.

De Carvalho, H.P., Huang, J., Zhao, M., Liu, G., Dong, L. and Liu, X. (2015), "Improvement of Methylene Blue removal by electrocoagulation/banana peel adsorption coupling in a batch system", *Alexandria Eng. J.*, **54**(3), 777-786. https://doi.org/10.1016/j.aej.2015.04.003.

Dhong, C., Miller, R., Root, N.B., Gupta, S., Kayser, L.V., Carpenter, C.W., Loh, K.J., Ramachandran, V.S. and Lipomi, D.J. (2019), "Role of indentation depth and contact area on human perception of softness for haptic interfaces", *Sci. Adv.*, **5**(8), 5-7. https://doi.org/10.1126/sciadv.aaw8845.

Eddy, N O, Odoemelem, S.A. and Mbaba, A. (2006), "Elemental composition of soil in some dumpsites", *Electr.. J. Environ. Agric. Food Chem*, **5**(3), 1349-1365.

Eddy, N. O and Ameh, P.O. (2021), "Computational and experimental study on Tapinanthus bangwensis leaves as corrosion inhibitor for mild steel and Al in 0.1 M HCl", *Curr. Top. Electrochem.*, **23**, 45-62.

Eddy, N. O. and Garg, R. (2022), *CaO Nanoparticles: Synthesis and Applications in Water Remediation*, In *Handbook of Research on Green Synthesis and Applications of Nanomaterials*, IGI Global.

Eddy, N.O., Garg, R., Garg, R., Aikoye, A. and Ita, B.I. (2022), "Waste to resource recovery: Mesoporous adsorbent from orange peel for the removal of trypan blue dye from aqueous solution", *Biomass Convers. Biorefin.*, 1-19. https://doi.org/10.1007/s13399-022-02571-5.

Ekop, A.S. and Eddy, N.O. (2010), "Thermodynamic study on the adsorption of Pb2 and Zn2 from aqueous solution by human hair", *E-J. Chem.*, **7**(4), 1296-1303. https://doi.org/10.1155/2010/849239.

Garg, R., Garg, R., Thakur, A. and Arif, S.M. (2020), "Water remediation using biosorbent obtained from agricultural and fruit waste", *Mater. Today Proc.*, **46**, 6669-6672. https://doi.org/10.1016/j.matpr.2021.04.132.

Garg, R., Kumari, M., Kumar, M., Dhiman, S. and Garg, R. (2021), "Green synthesis of calcium carbonate nanoparticles using waste fruit peel extract", *Mater. Today Proc.*, **46**, 6665-6668. https://doi.org/10.1016/j.matpr.2021.04.124.

Garg, R., Rani, P., Garg, R. and Eddy, N.O. (2021), "Study on potential applications and toxicity analysis of green synthesized nanoparticles", *Turkish J. Chem.*, 1690-1706. https://doi.org/10.3906/kim-2106-59.

Guillonneau, G., Kermouche, G., Bec, S. and Loubet, J.L. (2012), "Determination of mechanical properties by nanoindentation independently of indentation depth measurement", *J. Mater. Res.*, **27**(19), 2551-2560. https://doi.org/10.1557/jmr.2012.261.

Hejri, Z., Hejri, M., Omidvar, M. and Morshedi, S. (2020), "A novel nanocomposite as adsorbent for formaldehyde removal from aqueous solution", *Adv. Nano Res.*, **8**(1), 1-11. https://doi.org/10.12989/anr.2020.8.1.001.

Jalu, R.G., Chamada, T.A. and Kasirajan, D.R. (2021a), "Calcium oxide nanoparticles synthesis from hen eggshells for removal of lead (Pb(II)) from aqueous solution", *Environ. Challeng.*, **4**, 100193. https://doi.org/10.1016/j.envc.2021.100193.

Jasper, E.E., Ajibola, V.O. and Onwuka, J.C. (2020), "Nonlinear regression analysis of the sorption of crystal violet and methylene blue from aqueous solutions onto an agro-waste derived activated carbon", *Appl. Water Sci.*, **10**(6), 1-11. https://doi.org/10.1007/s13201-020-01218-y.

Jayakaran, P., Nirmala, G.S. and Govindarajan, L. (2019), "Qualitative and quantitative analysis of graphene-based adsorbents in wastewater treatment", *Int. J. Chem. Eng.*, **2019**. https://doi.org/10.1155/2019/9872502.

Junejo, R., Jalbani, N.S., Kaya, S., Erkan, S., Marzouki, R. and Memon, S. (2021), "Equilibrium and computational chemical modelling studies for the removal of methyl orange and methyl red dyes from water using modified silica resin", *Int. J. Environ. Anal. Chem.*, 1-17. https://doi.org/10.1080/03067319.2021.1979534.

Kuśmierek, K. and Świątkowski, A. (2015), "The influence of different agitation techniques on the adsorption kinetics of 4-chlorophenol on granular activated carbon", *React. Kinet. Mech. Catal.*, **116**(1), 261-271. https://doi.org/10.1007/s11144-015-0889-1.

Lafi, R., Abdellaoui, L., Montasser, I. and Hafiane, A. (2020), "Removal of methyl orange from aqueous solution onto modified extracted cellulose from Stipa Tenacissima L", *Int. J. Environ. Anal. Chem.*, **102**(19), 8124-8140. https://doi.org/10.1080/03067319.2020.1845663.

Maringgal, B., Hashim, N., Tawakkal, I.S.M.A., Hamzah, M.H. and Mohamed, M.T.M. (2020), "Biosynthesis of CaO nanoparticles using Trigona sp. Honey: Physicochemical characterization, antifungal activity, and cytotoxicity properties", *J. Mater. Res. Technol.*, **9**(5), 11756-11768. https://doi.org/10.1016/j.jmrt.2020.08.054.

Mehr, M.R., Fekri, M.H., Omidali, F., Eftekhari, N. and Akbari-Adergani, B. (2019), "Removal of chromium (Vi) from wastewater by palm kernel shell-based on a green method", *J. Chem. Heal. Risks*, **9**(1), 75-86. https://doi.org/10.22034/jchr.2019.584177.1012.

Mekatel, E.H., Amokrane, S., Aid, A., Nibou, D. and Trari, M. (2015), "Adsorption of methyl orange on nanoparticles of a synthetic zeolite NaA/CuO", *Comptes Rendus Chim.*, **18**(3), 336-344. https://doi.org/10.1016/j.crci.2014.09.009.

Mirghiasi, Z., Bakhtiari, F., Darezereshki, E. and Esmaeilzadeh, E. (2014), "Preparation and characterization of CaO nanoparticles from Ca(OH)2 by direct thermal decomposition method", *J. Ind. Eng. Chem.*, **20**(1), 113-117. https://doi.org/10.1016/j.jiec.2013.04.018.

Miyah, Y., Lahrichi, A., Idrissi, M., Boujraf, S., Taouda, H. and Zerrouq, F. (2017), "Assessment of adsorption kinetics for removal potential of Crystal Violet dye from aqueous solutions using Moroccan pyrophyllite", *J. Assoc. Arab Univ. Basic Appl. Sci.*, **23**, 20-28. https://doi.org/10.1016/j.jaubas.2016.06.001.

Nasrollahzadeh, M., Sajjadi, M., Iravani, S. and Varma, R.S. (2021), "Carbon-based sustainable nanomaterials for water treatment: State-of-art and future perspectives", *Chemosphere*, **263**, 128005. https://doi.org/10.1016/j.chemosphere.2020.128005.

Odoemelam, S.A. and Eddy, N.O. (2009), "Studies on the use of oyster, snail and periwinkle shells as adsorbents for the removal of Pb2+ from aqueous solution", *E-Journal Chem.*, **6**(1), 213-222. https://doi.org/10.1155/2009/407549.

Odoemelam, S.A., Emeh, U.N. and Eddy, N.O. (2018), "Experimental and computational chemistry studies on the removal of methylene blue and malachite green dyes from aqueous solution by neem (Azadirachta indica) leaves ", *J. Taibah Univ. Sci.*, **12**(3), 255-265. https://doi.org/10.1080/16583655.2018.1465725.

Qian, L. and Zhao, H. (2018), "Nanoindentation of soft biological materials", *Micromachines*, **9**(12). https://doi.org/10.3390/mi9120654.

Rahman, M.T., Asadul Hoque, M., Rahman, G.T., Gafur, M.A., Khan, R.A. and Hossain, M.K. (2019), "Study on the mechanical, electrical and optical properties of metal-oxide nanoparticles dispersed unsaturated polyester resin nanocomposites", *Results Phys.*, **13**, 102264. https://doi.org/10.1016/j.rinp.2019.102264.

Ramesh, T.N., Kirana, D.V., Ashwini, A. and Manasa, T.R. (2017), "Calcium hydroxide as low cost adsorbent for the effective removal of indigo carmine dye in water", *J. Saudi Chem. Soc.*, **21**(2), 165-171. https://doi.org/10.1016/j.jscs.2015.03.001.

Ramli, M., Rossani, R.B., Nadia, Y., Banta Darmawan, T., Febriani, Saiful and Ismail, Y.S. (2019), "Nanoparticle fabrication of calcium oxide (CaO) mediated by the extract of red dragon fruit peels (Hylocereus Polyrhizus) and its application as inorganic-anti-microorganism materials", *IOP Conf. Ser. Mater. Sci. Eng.*, **509**(1). https://doi.org/10.1088/1757-899X/509/1/012090.

Safavi, B., Asadollahfardi, G. and Darban, A.K. (2017), "Cyanide removal simulation from wastewater in the presence of Titanium dioxide nanoparticles", *Adv. Nano Res.*, **5**(1), 27-34. https://doi.org/10.12989/anr.2017.5.1.027.

Senthil Kumar, P., Fernando, P.S.A., Ahmed, R.T., Srinath, R., Priyadharshini, M., Vignesh, A.M. and Thanjiappan, A. (2014), "Effect of temperature on the adsorption of methylene blue dye onto sulfuric acid-treated orange peel", *Chem. Eng. Commun.*, **201**(11), 1526-1547. https://doi.org/10.1080/00986445.2013.819352.

Sharma, R., Garg, R. and Kumari, A. (2020), "A review on biogenic synthesis, applications and toxicity aspects of zinc oxide nanoparticles", *EXCLI J.*, **19**, 1325. https://doi.org/10.17179/excli2020-2842.

Soomro, M.Y., Hussain, I., Bano, N., Broitman, E., Nur, O. and Willander, M. (2012), "Nanoscale elastic modulus of single horizontal ZnO nanorod using nanoindentation experiment", *Nanosc. Res. Lett.*, **7**, 1-5. https://doi.org/10.1186/1556-276X-7-146.

Suk, J.W., Piner, R.D., An, J. and Ruoff, R.S. (2010), "Mechanical properties of monolayer graphene oxide", *ACS Nano*, **4**(11), 6557-6564. https://doi.org/10.1021/nn101781v.

Thakur, A., Punia, P., Dhar, R., Aggarwal, R. K. and Thakur, P. (2022), "Separation of cadmium and chromium heavy metals from industrial wastewater by using Ni-Zn nanoferrites", *Adv. Nano Res.*, **12**(5), 457-46. https://doi.org/10.12989/anr.2022.12.5.457

Vahdat, A., Ghasemi, B. and Yousefpour, M. (2020), "Mechanical properties of the hydroxyapatite and magnetic nanocomposite of hydroxyapatite adsorbents", *South African J. Chem. Eng.*, **33**, 90-94. https://doi.org/10.1016/j.sajce.2020.05.007.

Wu, L., Liu, X., Lv, G., Zhu, R., Tian, L., Liu, M., Yuxin Li, Rao, W., Liu, T. and Liao, L. (2021), "Study on the adsorption properties of methyl orange by natural one-dimensional nano-mineral materials with different structures", *Sci. Rep.*, **11**(1), 1-11. https://doi.org/10.1038/s41598-021-90235-1.

Yoonus, J., Resmi, R. and Beena, B. (2020), "Greener nanoscience: Piper betel leaf extract mediated synthesis of CaO nanoparticles and evaluation of its antibacterial and anticancer activity", *Mater. Today Proc.*, **41**, 535-540. https://doi.org/10.1016/j.matpr.2020.05.246.

Yunusa, U., Usman, B. and Bashir, M. (2021), "Experimental and quantum chemical investigation for the single and competitive adsorption of cationic dyes onto activated carbon", *Alger. J. Eng. Technol.*, **04**, 7-21.

JL